Fusion Engineering and Design 220 (2025) 115319

Contents lists available at ScienceDirect

Fusion Engineering and Design

journal homepage: www.elsevier.com/locate/fusengdes

Nanomechanical property and microstructural changes of tungsten Langmuir probes retrieved from JET with metal walls

E. Fortuna-Zalesna [a], M. Spychalski [a,*], P. Petersson [b], M. Rubel [b,c], A. Widdowson [d], B. Thomas [d], D. Moszczyńska [a], P. Wiecinski [a], Ł. Ciupiński [a], J. Likonen [e], R. Kerr [d], JET Contributors[1]

[a] Warsaw University of Technology, 02-507 Warsaw, Poland
[b] KTH Royal Institute of Technology, SE-1044 Stockholm, Sweden
[c] Uppsala University, Department Physics and Astronomy, Uppsala, Sweden
[d] UKAEA, Culham Campus, Abingdon, OX14 3DB, United Kingdom
[e] VTT Technical Research Centre of Finland, Otakaari 3 J, 02150 Espoo, Finland

ARTICLE INFO

Keywords:
Tungsten
Recrystallization
Nanoindentation
Langmuir probe
JET-ILW
IBA

ABSTRACT

Three tungsten Langmuir probes retrieved from the JET tokamak with the ITER-Like Wall (JET-ILW) from the bulk tungsten Tile 5 have been studied. Nano-indentation, microscopy, ion beam analysis (IBA), and X-ray diffraction were used to assess changes in their mechanical properties, microstructure, and phase composition. Four regions of the probes were studied - the tip and the base, at two sides: front and back. The hardness value of one of the probes (no. 5, Stack B) in the tip area was reduced when compared to the value measured on the base section: 5.4 GPa versus 8.8 GPa, respectively. On the two other probes, the hardness was similar to that of the reference material. At the protrusion of probe 5, the recrystallized zone was observed. The IBA analysis revealed that the probes' surfaces below the tips were covered by a thin layer of deposit composed primarily of beryllium, oxygen, carbon, and hydrogen isotopes, along with smaller amounts of nickel, nitrogen, and helium at some locations. The presence of tungsten carbide W_2C was revealed on the tip of probe 5, in the area where IBA measurements indicated elevated carbon content in the material, demonstrated by analysis of the XRD records.

1. Introduction

As decided by the ITER Organization, tungsten (W) was selected as the only candidate for plasma-facing components (PFCs) for the ITER and potentially future fusion reactors. Therefore, works related to structural changes of bulk tungsten components operating under reactor conditions are of particular interest, namely grain size change due to recrystallization, and modifications of the near-surface structure by re-deposition, fuel retention, and radiation effects. Equally important are issues related to the surface roughening projecting the erosion rate, or damage formation, which has a direct impact on the lifetime of components. In the case of tungsten, changes resulting from recrystallization are of special interest since they have a direct impact on the strength, hardness, and ductile to brittle transition temperature, and – in a consequence - on power handling capabilities and the PFCs lifetime [1, 2].

Due to the limited amount of material to be tested, it is not possible to determine the mechanical properties of these components using standard methods such as static tensile test. For this reason, other alternative/substitutive techniques are used, such as hardness measurements [3] or the determination of grain size on metallographic samples [e.g., EBSD (electron backscatter diffraction) maps] [4]. In turn, due to the challenges associated with changes in materials' properties in the thin near-surface zone, it is necessary to reach for techniques enabling analyses of mechanical properties in thin films/layers. Such a technique is the instrumented nano-hardness (IN) developed in the eighties by Doerner and Nix and refined by Oliver and Pharr [5], which made it possible to obtain hardness and Young's modulus values by analyzing the force-depth curve obtained during the load-unload cycle.

The IN method was applied in the present work to determine the changes in mechanical properties of tungsten Langmuir probes from the JET reactor. The objectives of this work cover the following issues: (i)

* Corresponding author.
E-mail address: maciej.spychalski@pw.edu.pl (M. Spychalski).
[1] See the author list in: E. Joffrin et al., Nucl. Fusion 59 (2019) 112021.

https://doi.org/10.1016/j.fusengdes.2025.115319
Received 10 December 2024; Received in revised form 23 May 2025; Accepted 4 July 2025
Available online 14 July 2025

determination by nanoindentation of the changes in mechanical properties of tungsten components after long-term exposure in JET; (ii) evaluation of the modification of the surface and sub-subsurface structure of such PFC, and (iii) assessment of the re-deposition in remote areas.

2. Experimental

Langmuir probes are the most common diagnostic tools for studies of the SOL plasma in tokamaks, they are used to determine electron temperature, floating potential, and ion density. All JET tungsten probes were produced by sintering and then subjected to rolling. Fig. 1a shows the bulk tungsten divertor module (Tile 5) with the probes placed in a gap between the tiles.

The study was conducted on three Langmuir probes exposed during two ITER-like wall (ILW) campaigns from 2011 to 2014. All probes were removed from the JET divertor after the second campaign from module 16 W, Tile 5. Tile 5 consists of four stacks, marked with the letters A-D, each stack consisting of 24 bulk tungsten lamellae. The outer strike point in JET was mainly located on Stacks C and D and rather seldom on B. Probe no 1 was mounted at Stack A, while probes no 3 and 5 at Stack B. All probes have the same geometry, as shown in Fig. 1b

During these two campaigns, the probes experienced 27.2 h of X-point operations. The location of the outer strike point during the first campaign was predominantly on Tile 5, while during the second one on Tile 6. Strike point distributions (including Tile 5) are shown in [6]. However, it should be emphasized that the first campaign contained a smaller number of high-power pulses in comparison to the second one, which was focused on high-power plasma scenarios. It's essential to add that the second campaign ended with 300 discharges fuelled with hydrogen. Detailed information on campaigns can be found in [6,7].

The cumulative fluence for the time the Langmuir probes were in the vessel (JET pulse numbers 79,854–87,944, indicating the beginning of the first ILW campaign and the end of the second one) has been calculated. For probes 1, 3, and 5, these were 4.39×10^{23}, 1.02×10^{24}, and 2.49×10^{24} particles/m^2, respectively.

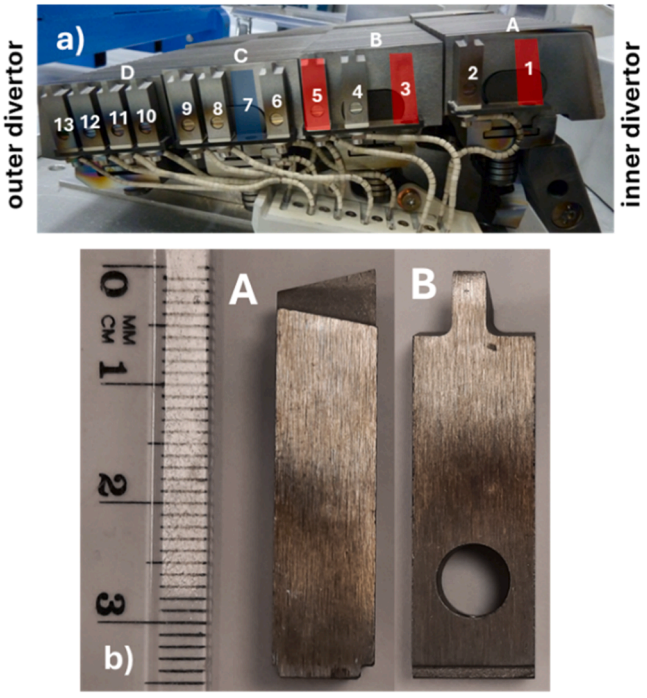

Fig. 1. (a) Arrangement of Langmuir probes at Tile 5 of JET divertor; probes numbers are shown. (b) Image of probe no 5: A - side wall and B - plasma facing, front wall.

In the present work, for the determination of the mechanical properties of the probes by nanoindentation, we used procedures successfully implemented in our previous work [8]. All details regarding the principle of the method, experimental procedures (including calibration), and possible sources of errors are described there [8]. The present work contains nanoindentation results that were not affected by measurement errors due to the geometry of the samples, as was the case in the previous one. All the examined probes worked in the JET at Tile 5, had the same geometry and flat parallel walls and could be tested without generating measurement errors due to the attachment of the specimens prior to nanoindentation measurements. As in the previous study, the triboindenter model Hysitron Ti-900 was used for the tests.

Roughness measurements of the probes by optical profilometer showed for all probes high roughness values of 1.1–1.5 μm. For that reason, measurement sites with a flat surface were chosen each time based on observations of surface morphology in the scanning probe microscopy (SPM) mode. With this approach, the roughness of the areas selected for measurements was much smaller than that determined by the optical profilometer and ranged from 11 to 19 nm. To be able to image the sample surface in SPM mode, a smaller indenter and a force of 10 mN were applied. The results presented in the article are an average obtained from twenty valid measurements. The nano-hardness measurements were carried out in the area of the tip and in the support structure, referred to as the base in the work.

Scanning electron microscopy (Hitachi SU-8000 FE-SEM equipped with EDS, Energy Dispersive Spectrometer, Thermo Scientific enabling beryllium detection) was used to assess the surface modification of the probes, whereas the sub-surface structure of the probes was determined on the FIB (Focus Ion Beam) - produced cross-sections (Helios 5 FIB/SEM Thermo Fisher Scientific and FIB/SEM Hitachi NB5000). The phase composition was determined with a Bruker D8 Discover x-ray diffractometer working in a point beam geometry with a 1.5 mm collimator, using non-monochromatic CoK_α radiation. The measurements were taken in the 2θ range of 20°–130°, with step 0.02, and time per step of 8 s. The surface composition of probes was analyzed by time-of-flight heavy ion elastic recoil detection analysis (ToF-HIERDA) with a 44 MeV $^{127}I^{8+}$ beam. Measurements were taken on all probes, on each side surface, at four points along the length of the probes and with five measurements taken on the front side.

3. Results and discussion

3.1. Microstructural features

3.1.1. Surface morphology

Images showing typical probes' surfaces are provided in Fig. 2 on the example of probe no 3. Lines that are traces of material machining can be seen. The same surface characteristics have been recorded both in the protrusion region and the base.

A feature common to all samples was the presence of a dark pattern on the base part of the probes. It should be noted that it was present on all four sides of the probes, in their middle and bottom parts. The thin film on their surface consisted of the following elements: oxygen, nitrogen, carbon, and nickel, as documented by the energy-dispersive X-ray spectroscopy (EDX) spectra given in Fig. 3. A small peak originating from beryllium can be seen on the spectrum shown on a logarithmic scale. It should be noted that the energy of emitted X-rays is very low, $K_{\alpha(Be)} = 108$ eV, and this has an impact on the detection sensitivity. Moreover, in the image in Fig. 2b registered in BSE mode, one can clearly notice stronger redeposition in the surface grooves. In all cases, no signs of re-melting were found at the base parts. At this point, it should be mentioned that the presence of a deposit on the base part of the Langmuir probes was also found in earlier works for probes mounted at Tiles 3 and 6 of the JET divertor [8,9]. The surface morphology of those probes was analogous to that observed in the present work, despite their different geometry.

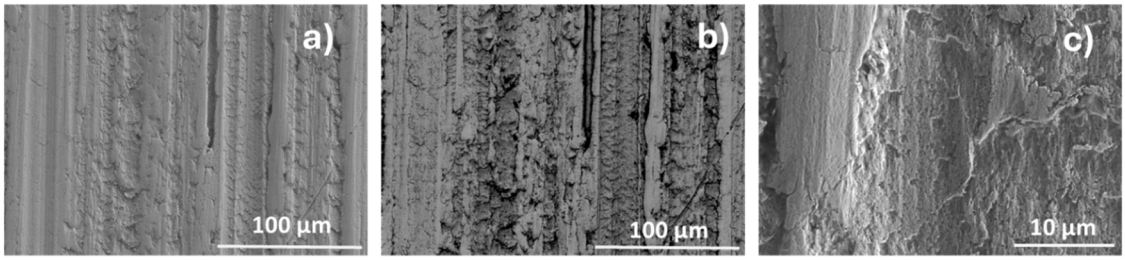

Fig. 2. SEM images of the base part of probe no 3: (a, c) SE, secondary electron and b) BSE, backscattered electron mode.

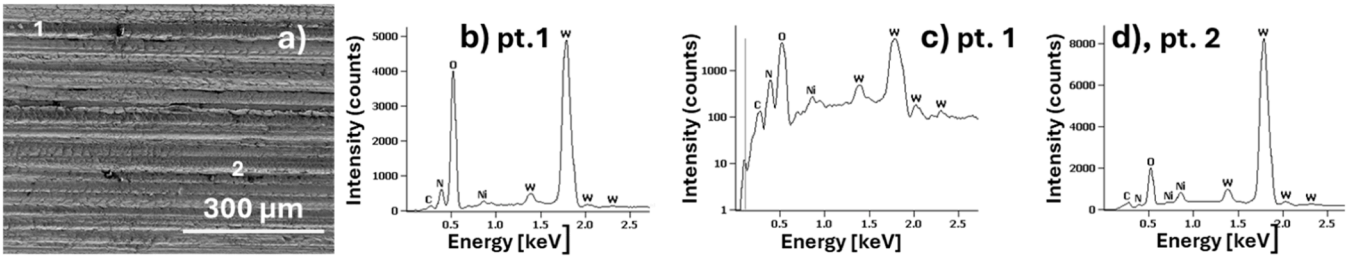

Fig. 3. SEM image of the base structure (a) together with the EDX (Energy-Dispersive X-ray) spectra from the groove (b-c) and the ridge (d), probe no 1. In Figure c, the line shows the position of the beryllium peak.

Observations made with the bare eye showed no melt damage on the tips of any of the probes. However, some damage was detected in their tip area during microscopic observations. The probes no 1 and 3 showed cracks and chipping at the tip edge, as exemplified in Fig. 4. For these probes, damage was, however, limited to the top zone of the tip. In the case of probe no 5, the situation was somewhat different. SEM observations revealed below its tip end a large re-crystallized zone, ca. 1.3 mm in size, with clearly visible grain boundaries of the order of 100 µm, Fig. 5 ab. Below this zone, in the middle part of the tip, overheated material was found with visible pores and locally with re-solidified droplets, Fig. 5c.

3.1.2. *Sub-surface structure*

Observations made on the FIB-produced cross-sections provided a detailed insight into the internal structure of the probes' subsurface zones. Images of the subsurface structure of the base and the overheated zone present at the tip of probe no 5, just below the zone with clearly visible grain boundaries, are presented in Figs. 6 and 7, respectively. Results in Fig. 6 show the presence of a zone with strong plastic deformation at the base surface, up to 3 µm thick, both at its front and back sides. Beneath it, in the case of the cross-section made on the back side, small grains of a few to 10 µm were observed. A larger cross-section made on the front side reveals a more complex image, however, also over a larger area, grains of similar size to those revealed on the cross-section made on the back side are visible. A heavily deformed zone is often observed in plastically deformed materials - e.g., sheet metal, the so-called "surface deformed zone". It can also be formed in the material due to surface treatment, such as grinding. Its presence on the surface of the material, which was plastically deformed, in this case rolled, is not surprising. As seen in Fig. 7, no surface deformed zone is observed anymore on the surface in the tip region. Within the cross-section, several large, equiaxed grains, with a size of the order of 40 µm, can be seen. This is a typical structure for recrystallized material. In summary, FIB-produced cross-sections clearly indicated the transformation of the subsurface structure in the tip region of probe no 5. Although these changes cannot be seen as clearly as in the EBSD maps or in the etched metallographic samples [4,9,10], they are well enough documented to conclude the modification of the grain boundary structure by recrystallization.

Changes in grain structure with respect to Langmuir probes were found in previous studies [8,9]. The presence of the recrystallized zone in tungsten PFCs was also reported in studies of other tungsten PFCs [3, 11].

3.1.3. *Deposition in shadowed areas*

Visual inspection indicated the presence of thin deposited layers on the base part of the probes. The re-deposition was not limited to the plasma-facing sides but occurred on all four sides of the probes. The tip and the base part just below it were clean, most likely due to plasma exposure. The results of the Langmuir probe analysis with ToF HIERDA are given in Fig. 8. The IBA analysis revealed that the probes' surface was covered by a thin film containing primary oxygen, beryllium,

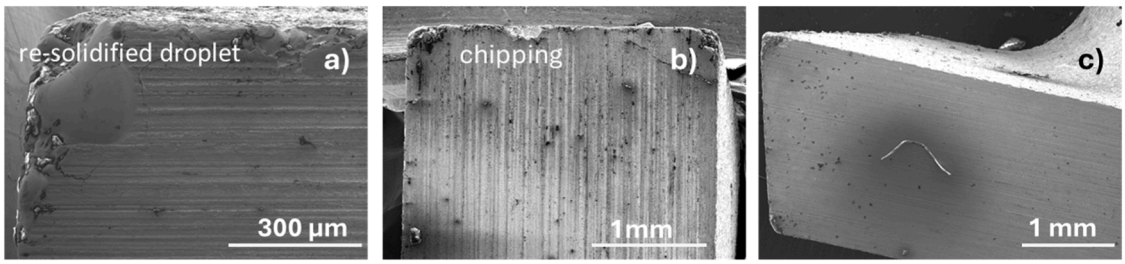

Fig. 4. SEM images of the tip end: a) probe no 1, b) probe no 3 and c) unexposed probe. On the tip of the unexposed probe, no signs of cracking, melting, or recrystallization are observed. Visible chipping of material on corners.

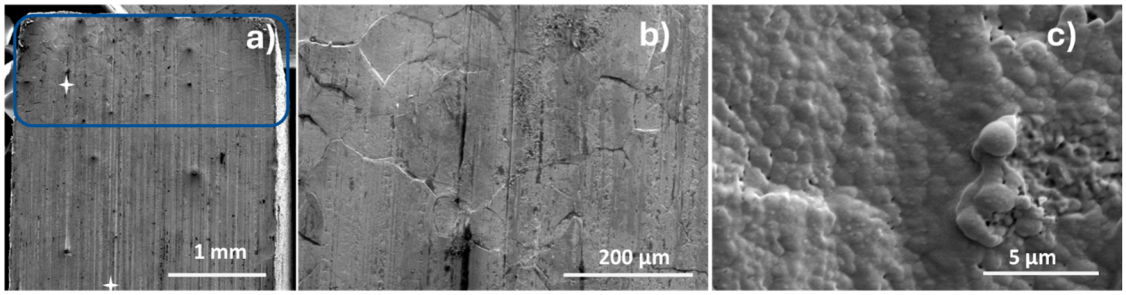

Fig. 5. SEM images of probe no 5 tip: (a-b) recrystallized zone, c) middle part of the tip, 2.7 mm from the tip end. The locations where images 5b and 5c were recorded are marked in Fig. 5a with asterisks.

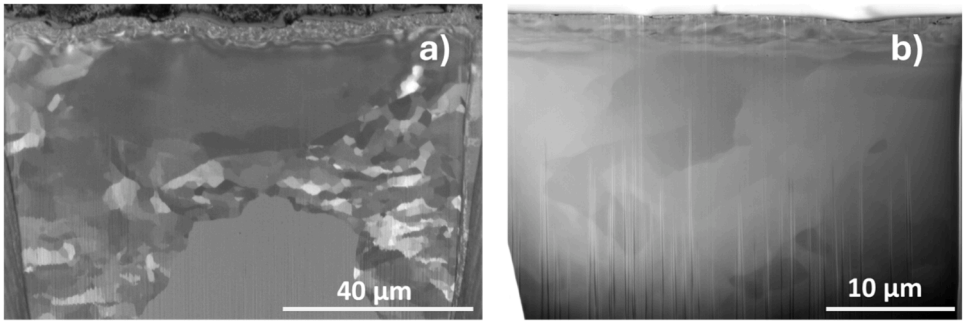

Fig. 6. SEM images of FIB cross-sections of probe no 5 base part: a) front and b) back side. The cross-section on the front wall was made at a distance of 12.6 mm from the base's upper edge.

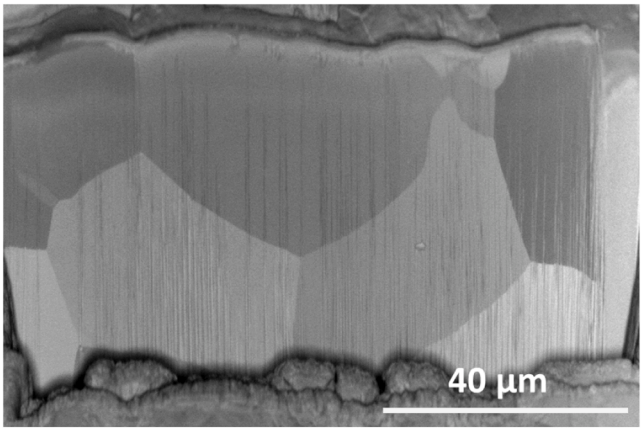

Fig. 7. SEM image of FIB cross-section of probe no 5 tip region (1.65 mm from the tip end).

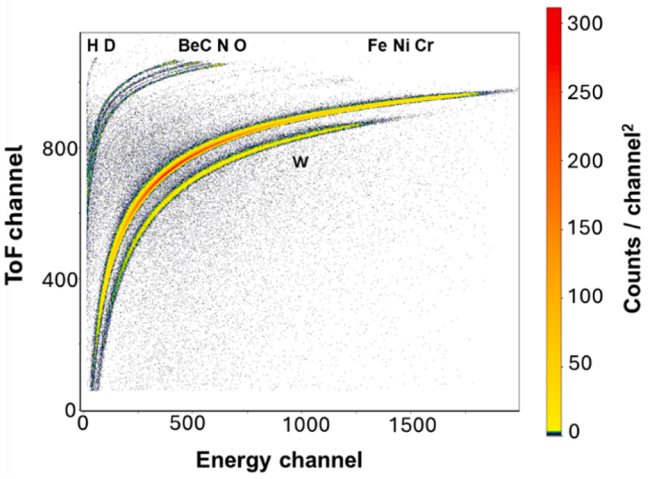

Fig. 8. Results of the Langmuir probe analysis with ToF HIERDA - spectrum with described detected elements; probe no 5, sidewall, the bottom part of the base (the closest point to zero in Fig. 9).

carbon, and hydrogen isotopes, along with smaller amounts of the components of Inconel, nitrogen, and, at some locations, helium.

The distribution of elemental content of the deposit along the length of the probes, including hydrogen isotopes, is shown in Fig. 9, using the front wall as an example. The results obtained confirm that re-deposition takes place in the area with a black tarnish located on the base part of the probes, visible in the images in Fig. 1b What breaks out of this pattern is the distribution of carbon. In this case, its maximum content is recorded in the area without visible tarnish. Beryllium and oxygen are the major species. Their amount is similar in most co-deposits. The presence of nitrogen used for plasma edge cooling is clear. Its presence in the deposits, as well as in the dust particles forming in the JET reactor, has been reported before [12–14]. A similar observation can be made with regard to the earlier results of the work carried out at the ASDEX-Upgrade [15,16]. The contribution of Inconel constituents is noticeable as well. Their origin on the probes is mainly related to the erosion of the vacuum vessel wall [17]. The erosion of the Inconel alloy ICRF (the ion cyclotron range of frequencies) antenna grill and the melting of the tie rods in the divertor Tile 7 may also have contributed to the elevated nickel content [17].

The profiles in Fig. 9 show the high hydrogen signal, reflecting the fact that the ILW-2 ended with the hydrogen campaign, which resulted in the depletion of the deuterium content in deposits [18,19]. Results of point nuclear reaction analysis (NRA) on the surface of probe 26, detached from Tile 6 of the JET divertor similarly after the first two ILW campaigns, presented in [9], show that deuterium was at the level of 10^{15} atoms/cm^2. Additionally, low concentrations of beryllium and other elements originating from the erosion of in-vessel components

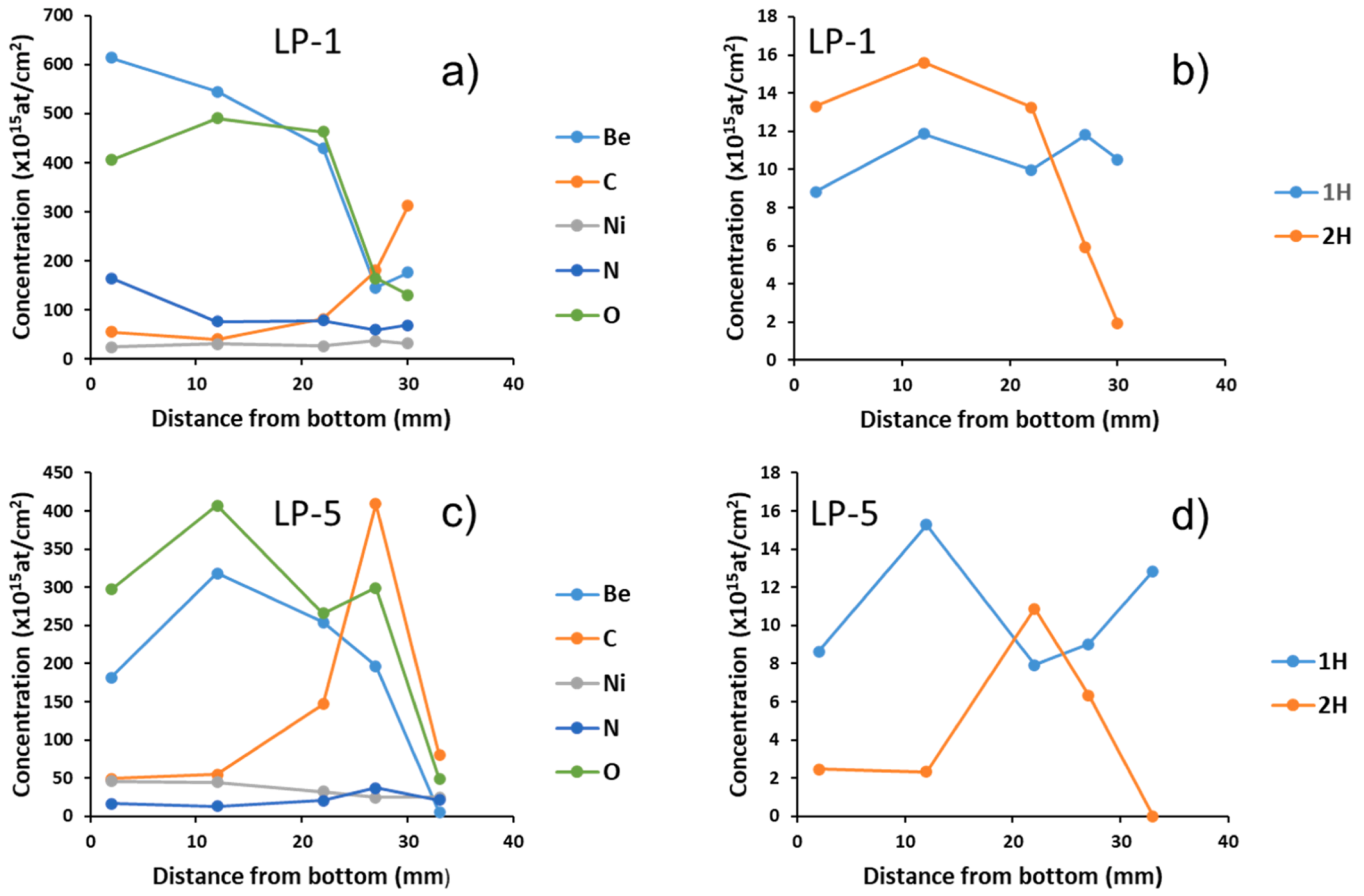

Fig. 9. Distribution of Be, C, Ni, N, O (a, c) and hydrogen isotopes (b, d) along the length of probes no.1 and 5, front side.

were detected in the paper cited. These results are consistent with those presented in our work.

The profiles of helium are not depicted. He (^{3}He and ^{4}He) was detected only in a few points, mostly on the sides. Its content was at the level from several to twenty x 10^{15}at/cm^2. Since the amount of helium gas injected into the JET chamber for 2011–2014 (10^{23} ^{4}He + ^{3}He) was four orders of magnitude higher than the number of helium ions produced by the D-D fusion reaction (2.9 × 10^{19} 0.82 MeV ^{3}He ions), any helium detected should be assigned to gas injection [9].

It should be mentioned here that deposition has been detected in the plasma-shadowed regions of the JET reactor. Beryllium-rich deposits on the test mirrors and quartz microbalance [20], thin films in the gaps separating adjacent lamellae in Tile 5 and in castellated structures [19, 21], or deposition in the remote corners of Tiles 4 and 6 [22] are just some examples. These deposits contain mainly beryllium with the addition of carbon, oxygen, and deuterium. They may pose a potential hazard due to their contribution to fuel retention, an issue of concern from the standpoint of tritium inventory.

3.1.4. Phase composition

XRD patterns collected from the two regions of probe no 5, on the bottom part of the tip and on the base part, in the zone covered by a thin layer of re-deposited matter, are presented in Fig. 10. The measurement location can be seen in Fig. 11 as the illuminated area. No other phases than tungsten were detected in the base part of the probe, whereas the diffraction pattern recorded at the lower part of the tip revealed the presence of the W_2C (tungsten carbide) phase. It is also worth noting that the location where the carbides were found coincides with the area where elevated carbon content was detected during the IBA analysis. The presence of tungsten carbides had already been confirmed on the surfaces of tungsten plasma-facing components retrieved from JET

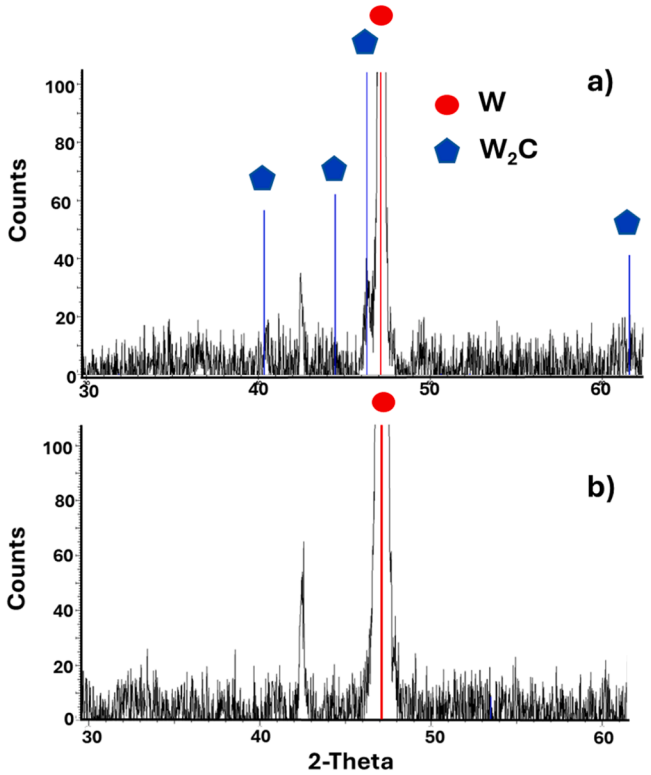

Fig. 10. XRD pattern for: a) tip and b) base of probe no 5.

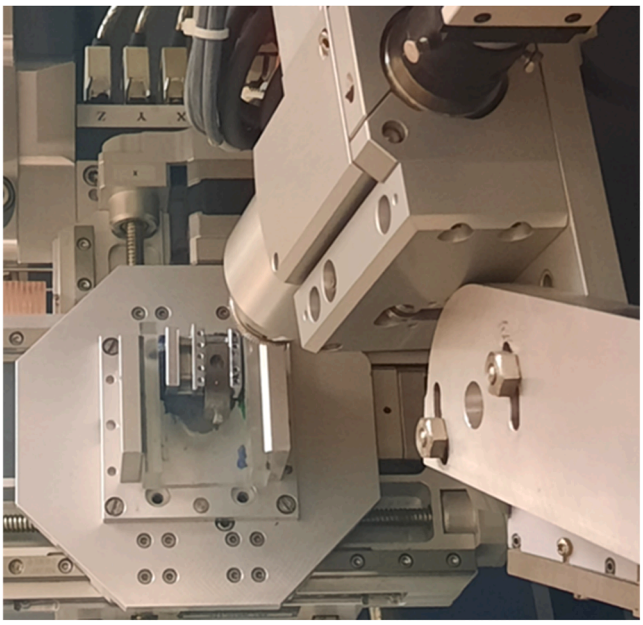

Fig. 11. Photograph showing sample mounting in the X-ray diffractometer.

tokamak [23]. The formation of the W_2C phase was also proved during our previous research on Langmuir probes [8].

3.2. Mechanical properties

The results of nano-indentations of the tips and base parts of all probes, as well as a probe that was not placed in the device, are given in Table 1 and Fig. 12. A summary of all representative force-displacement curves, as shown in Fig. 13, provides additional insight into the results obtained.

The result that draws attention to itself is the reduced hardness value of the probe no 5 in the tip area (5.4 GPa) on the front side, compared to the hardness value measured on the base section (8.8 GPa). The hardness values from the back (B) side of this probe were similar to that measured on the front side in the base part. The differences in hardness on the base and tip of probes no 1 and no 3 were small, and their values were comparable to the unexposed sample (8.5 GPa).

Looking at the column diagram in Fig. 12 and the representative force-displacement curves in Fig. 13, it is clear that the only area whose properties deviate from the average is the tip of probe no 5. This result suggests a degradation of the material's mechanical properties in this area, which may be related to recrystallization of the material (which was confirmed in this case by cross-sections made using the FIB technique).

As shown in Chapter 3.1.2, the area in the direct vicinity of the probe surface is heavily deformed; such a zone is often observed in plastically deformed materials - e.g., sheet metal, the so-called "surface deformed zone." Therefore, in relation to our results, we must refer to work carried out on a deformed material. ITER grade tungsten was studied in [10] to deduce the impact of plastic deformation on the hardness. In the case of the work cited above, the hardness at room temperature for recrystallized material (with a mean grain size of 36 μm) amounted to about 6.7 GPa compared to 8.4 GPa for the as-forged state. Literature data for the tungsten nano-hardness can be found in [24]; it is in the range of 3.5–5.8 GPa for a recrystallized state.

Table 1
Results of nano-hardness measurements.

		Nanohardness, H [GPa]		
		Average(H)	SD (H)	Error (H)
Probe no 1	tip	8.4	0.3	0.1
	base	9.8	0.6	0.2
Probe no 3	tip	9.1	0.7	0.1
	base	9.6	0.6	0.1
Probe no 5	tip	5.4	0.3	0.1
	base	8.8	0.3	0.1
	tip, side B*	8.8	0.8	0.2
	base, side B	9.4	0.7	0.2
initial state	base	8.5	0.9	0.2

*back side.

The results presented in this paper do not deviate from literature data on tungsten, making them reliable and allowing us to conclude that the nanoindentation technique can be successfully applied to control changes in the surface mechanical properties of tungsten components. Furthermore, the results clearly document a high agreement in the mechanical properties of the single probes mounted in the divertor area. The above statement refers to the material which has not undergone structural changes/transformation during operation. Both the hardness values and the recorded force-depth curves are characterized by small scatter values.

The differences in nano-hardness between the tip and base of probe no 5 are due to the grain growth that has occurred in the protrusion area, as confirmed by the sub-surface structure studies presented in Section 3.1.2. The plasma strike point distributions in the JET divertor during the first two ILW campaigns presented in [6] show that the outer strike point was mainly located on Stacks C and D, seldom on B. The lack of structural changes on probe no 1, mounted at Stack A, and probe no 3, located relatively close to Stack A, is therefore understandable. The situation is different for probe no 5. Its location at the boundary with the C-stack undoubtedly had an impact on cumulative particle fluence and, consequently, on changes in the near-surface structure. These considerations are confirmed by the cumulative fluence values for these probes given in the Experimental section, which were the lowest for probe no 1 and the highest for probe no 5.

4. Summary

The present work has extended the knowledge of changes in the mechanical properties and degradation of Langmuir probes operating in the JET reactor environment. The work emphasized three main issues, which are: (i) analyses of mechanical data for tungsten components influenced by heat loads, (ii) modification of their surface and sub-subsurface structure, and (iii) re-deposition in remote areas. The most significant result from the point of view of evaluating the changes in the mechanical properties of the probes' material was that nano-hardness measurements revealed differences in the value of this parameter between the tip and the base section of one of the probes tested (5.4 vs. 8.8 GPa, respectively), which experienced the highest cumulative fluence. Interestingly, all other probes, irrespective of where they were measured, had hardness values similar (8.5 GPa) to the reference probe that did not operate in the device and did not experience heat loads.

Observations of the probe morphology and its near-surface structure on FIB cross-sections revealed the modification of the grain boundary structure caused by recrystallization. Another noteworthy result is the formation of a tungsten sub-carbide phase in the tip, in the area where IBA measurements indicated elevated carbon content in the material, which was demonstrated by analysis of the XRD records. In turn, the IBA analysis revealed that the probes' surfaces below the tips were covered by a film of deposit composed primarily of oxygen, beryllium, carbon, and hydrogen isotopes, along with smaller amounts of Inconel components, nitrogen, and helium at some locations. Whereby the re-deposition was not restricted to the plasma-facing sides but occurred on all four sides of the probes.

The added value of this work is that it presents a complete procedure that can be successfully used to assess the surface changes of tungsten components after operation in fusion devices. The advantage of this procedure is that we do not modify the test samples in any way, before or

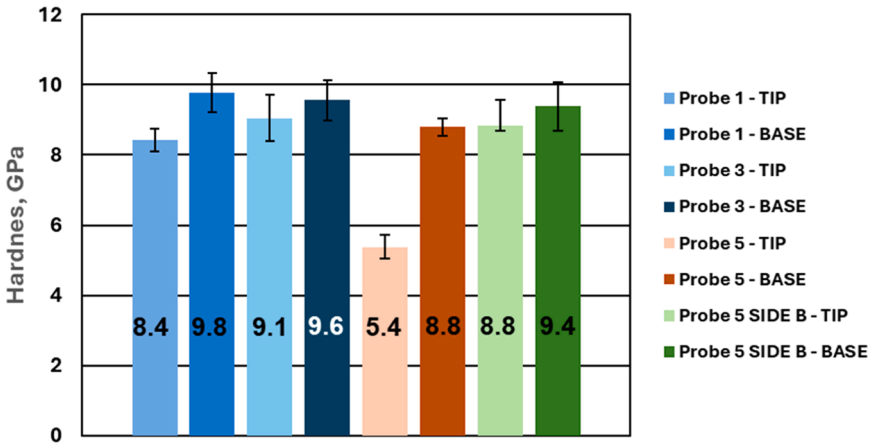

Fig. 12. Results of nano-hardness measurements of probes no 1, 3 and 5.

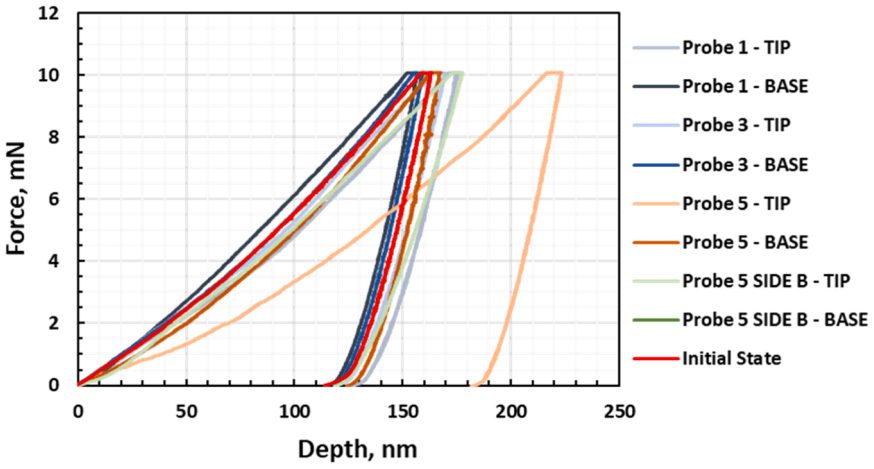

Fig. 13. Representative force-displacement curves for all measurement sites.

during mechanical nano-indentation tests. Measurements are made directly on the original surface of the probes. After the measurements, they are in the same condition as they were before. Therefore, the samples can be used to carry out further examinations, including destructive ones, if required. In addition, if a reliable database relating to the surface properties of the components in their initial state is available, changes that may appear in their near-surface zone can be tracked. And just as importantly, this method does not require a large amount of material.

It is beyond dispute that the mechanical properties and microstructure of the sub-surface region of the tungsten plasma-facing components will play an extremely important role in their performance. Accordingly, the surface finish should be an issue that needs to be considered when procuring components for ITER and future fusion devices, which was not the case for the W coatings. This is important not only because of the potential recrystallization or damage formation but also because the number of defects present in the material's structure can affect fuel retention.

CRediT authorship contribution statement

E. Fortuna-Zalesna: Writing – review & editing, Investigation, Conceptualization, Visualization. **M. Spychalski:** Methodology, Investigation, Formal analysis, Conceptualization, Writing – review & editing, Visualization. **P. Petersson:** Investigation, Formal analysis, Visualization. **M. Rubel:** Supervision. **A. Widdowson:** Resources, Validation. **B. Thomas:** Validation. **D. Moszczyńska:** Investigation. **P. Wiecinski:** Investigation. **Ł. Ciupiński:** Project administration, Writing – review & editing. **J. Likonen:** Project administration. **R. Kerr:** Investigation.

Declaration of competing interest

The authors declare that they have no known competing financial interests or personal relationships that could have appeared to influence the work reported in this paper.

Acknowledgments

This work has been carried out within the framework of the EUROfusion Consortium, funded by the European Union via the Euratom Research and Training Programme (Grant Agreement No 101052200 — EUROfusion). Views and opinions expressed are however those of the author(s) only and do not necessarily reflect those of the European Union or the European Commission. Neither the European Union nor the European Commission can be held responsible for them. This work has been partially supported by the Ministry of Science and Higher Education of Poland from financial appropriations for science of the year 2024, granted for the implementation of the international co-financed project.

Data availability

No data was used for the research described in the article.

References

[1] ITER, technical report_no_ITR-18-003 ITER Research Plan within the Staged Approach 2018 Chapter Tungsten Related, Material Issues 45. 2018.
[2] A. Suslova, et al., Recrystallization and grain growth induced by ELMs-like transient heat loads in deformed tungsten samples, Sci. Rep. 4 (1) (2014) 6845, https://doi.org/10.1038/srep06845.
[3] G. Pintsuk, et al., Metallography and mechanical parameters of plasma-exposed plasma-facing materials and components, Phys. Scr. T171 (2020) 014042.
[4] X. Xiao, et al., High temperature nano-indentation of tungsten: modelling and experimental validation, Mater. Sci. Eng. A 743 (2019) 106.
[5] W.C. Oliver, G.M. Pharr, An improved technique for determining hardness and elastic modulus using load and displacement sensing indentation experiments, J. Mater. Res. 7 (1992) 1564.
[6] K. Heinola, et al., Experience on divertor fuel retention after two ITER-Like Wall campaigns, Phys. Scr. T170 (2017) 014063.
[7] A. Lahtinen, et al., Deuterium retention in the divertor tiles of JET ITER-Like wall, Nuclear Mater. Energy 12 (2017) 655–661.
[8] M. Spychalski, et al., Tungsten Langmuir probes from JET-with the ITER-Like Wall: assessment of mechanical properties by nano-indentation, Phys. Scr. 96 (2021) 124072.
[9] R. Kerr, et al., Mechanical and microstructural analysis of tungsten exposed in JET deuterium plasmas, Nucl. Mate. Energy 35 (2023) 101420.
[10] D. Terentyev, et al., High temperature nanoindentation of tungsten: modelling and experimental validation, Int. J. Refract. Metals Hard Mater. 89 (2020) 105222.
[11] J. Coenen, et al., Transient induced tungsten melting at Joint European Torus (JET), Phys. Scr. T170 (2017) 014013.
[12] M. Rubel, et al., Dust generation in tokamaks: overview of beryllium and tungsten dust characterisation in JET with the ITER-like wall, Fusion Eng. Des. 136 (2018) 579–586.
[13] P. Strom, et al., Analysis of deposited layers with deuterium and impurity elements on samples from the divertor of JET with ITER-like wall, J. Nucl. Mater. 516 (2019) 202.
[14] E. Fortuna-Zaleśna, et al., Dust generation and accumulation in JET-ILW: morphology and stability of co-deposits on main plasma-facing components and wall probes, Phys. Scr. 96 (2021) 124038.
[15] G. Meisl, et al., Nitrogen retention in ASDEX Upgrade, J. Nucl. Mater. 463 (2015) 668.
[16] E. Fortuna-Zalesna, et al., Post mortem analysis of a tungsten coated tile from the outer divertor strike point region of ASDEX upgrade, Nucl. Mater. Energy 9 (2016) 128–131.
[17] A. Widdowson, et al., Deposition of impurity metals during campaigns with the JET ITER-like Wall, Nucl. Mater. Energy 19 (2019) 218–2024.
[18] A. Widdowson, et al., Overview of fuel inventory in JET with the ITER-like wall, Nucl. Fusion. 57 (2017) 086045.
[19] M. Rubel, et al., Fuel inventory and deposition in castellated structures in JET-ILW, Nucl. Fusion. 57 (2017) 066027.
[20] P. Petersson, et al., Co-deposited layers in the divertor region of JET-ILW, J. Nucl. Mater. 463 (2015) 814–817.
[21] M. Tokitani, et al., Co-deposited layers on gap surfaces of bulk tungsten divertor tiles in JET ITER-like wall: directional effects and nanostructures, Nucl. Mater. Energy 39 (2024) 101678.
[22] N. Catarino, et al., Deposition in the tungsten divertor during the 2011–2016 campaigns in JET with ITER-like wall, Phys. Scr. 2020 (2020) 014044.
[23] A. Lagoyannis, et al., Surface composition and structure of divertor tiles following the JET tokamak operation with the ITER-like wall, Nucl. Fusion. 57 (2017) 076027.
[24] H. Huang, Y.Q. Wu, S.L. Wang, Mechanical properties of single crystal tungsten microwhiskers characterized by nanoindentation, Mater. Sci. Eng. A 523 (2009) 193.